Rock Mechanics and Rock Engineering (2023) 56:1387–1398
https://doi.org/10.1007/s00603-022-03146-6

ORIGINAL PAPER

Experimental and Theoretical Study on the Creep Behavior of a Clayey Rock

Hongdan Yu[1] · Weizhong Chen[1] · Yongshang Ma[1] · Xianjun Tan[1] · Jianping Yang[1]

Received: 11 May 2022 / Accepted: 1 November 2022 / Published online: 18 November 2022

Abstract

An understanding of the creep behavior of clayey rocks is considered fundamental for further development in the fields of nuclear waste underground disposal, underground mine design, strata control, and many other geological phenomena occurring in the earth's crust. In this research, we performed a series of long-term triaxial compressive tests on a typical clayey rock, which confirmed its high creep potential beyond the creep threshold. Further analysis of the creep mechanism of this clayey rock indicated that two effects—strengthening and damage—are accompanied by the creep process. Additionally, based on the overstress theory and Drucker–Prager cap model, we developed a novel constitutive model considering two creep reference surfaces—cohesion and consolidation. Meanwhile, laws to reflect the strength and damage effect during creep were established and applied to the above constitutive model. Finally, the above theoretical studies were implemented in the finite element method software ABAQUS FEA using the subroutines CREEP and USDFLD. Some theory parameters were verified through back analysis. A comparison between the experimental results and numerical simulations confirmed the superiority of the established theoretical model.

Highlights

- Clayey rock exhibits high creep potential beyond the creep threshold.
- Two effects—strengthening and damage—are accompanied by the creep process.
- A novel creep constitutive model was established.
- Strengthening and damage laws during creep were developed.
- Model numerical implementation and parameters determination.

Keywords Clayey rock · Creep behavior · Creep tests · Creep mechanism · Constitutive model

1 Introduction

Clayey rocks can be exposed to geological engineering activity, including nuclear waste geological disposal, slip zones within landslides, hydraulic engineering facilities, and the mining of deep mineral resources. Strong diagenesis during the sedimentary process causes the clayey rock to exhibit great differences in structure and texture (Zeng et al. 2008; Robinet et al. 2012; Desbois et al. 2017), making it a heterogeneous, discontinuous, and anisotropic geomedium. Rocks and clayey rocks, in particular, have a complicated mechanical behavior that is often time-dependent (Griggs 1939; Yang et al. 2014, 2015; Wang et al. 2020; Yu et al. 2021; Vu et al. 2021). In most cases, creep behavior occurs at low-stress levels; in accordance, large deformations can accumulate over long periods, increasing the possibility of slow and unconstrained failure. Many large-scale rock engineering projects have service lives of decades to hundreds of years or, in the case of nuclear waste disposal underground

✉ Hongdan Yu
yuhd_1013@163.com

✉ Weizhong Chen
wzchen@whrsm.ac.cn

[1] State Key Laboratory of Geomechanics and Geotechnical Engineering, Institute of Rock and Soil Mechanics, Chinese Academy of Sciences, Wuhan 430071, Hubei, China

infrastructures, even thousands of years. Hence, the creep properties of rock mass are fundamental to the development of a geological facility, from the initial construction and closure phases to the long-term system evolution, post-closure.

The creep behavior of clayey rocks has been extensively studied through laboratory experiments. Many scholars, like Arulanandan et al. (1972), Bonini et al. (2003), Gasc-Barbier et al. (2004), Zhang and Rothfuchs (2004), Fabre and Pellet (2006), Naumann et al. (2007), Yu et al. (2015, 2021), Zhang and Laurich (2020) and Shi et al. (2022), have conducted series of creep tests on different types of clayey rocks, including Boom Clay, Callovo-Oxfordian argillite, Opalinus Clay, and Bure clayey rock. Meaningful results were preliminarily obtained: those clayey rocks exhibited obvious creep phenomena; a stress threshold might exist, under which no creep was found; the excess pore water pressure generated during the creep process was mainly caused by secondary consolidation. The high creep potential of clayey rock was also observed in field measurements (Giraud and Rousset 1996; Neerdael et al. 1999; Kupferschmied et al. 2015). The creep process, together with excess pore pressure dissipation and stress redistributions near the excavations, may continually influence the development of the disturbed excavation zone.

Some scholars studied the creep phenomenon of clayey rock from a microscopic point of view (Pusch 1979; Fabre and Pellet 2006; Zhang et al. 2010; Zhao et al. 2020; Yu et al. 2021). Two phases, mobilization and rupture, were found within the creep process of clayey rock, during which the aggregates rotated and translated while a certain number of internal particle connections disintegrated. Two effects may occur in the creep process: strengthening and weakening. For the former, the particles translate and rotate under the action of force, often resulting in a more stable structure where the interparticle bonds are stronger but brittle, i.e., a strengthening effect. For the latter, under the action of long-term load, the existing micro-fissures continually develop, with the help of the gradual sprout micro-fissures inside the sample, and the clay structure is damaged, which is a weakening effect. Many scholars focused on the weakening phenomenon during the creep process for clayey rock, which was confirmed by many experiments, both in the laboratory (Fabre and Pellet 2006; Chang and Zoback 2009; Yu et al. 2021) and in situ measurements (Blümling et al. 2007; Kupferschmied et al. 2015). Meanwhile, some authors, like Liu et al. (2015) and Pusch et al. (2016), have noticed the strengthening phenomenon during creep. Liu et al. (2015) found that the mechanical strength of Callovo-Oxfordian argillite obtained in the triaxial phase after the one-step creep phase was increased compared to that of the normal triaxial test. Pusch et al. (2016) combined this strengthening effect with specific projects, pointing out that creep could strengthen clay and lead to stable conditions in very old clay slopes. However, to the authors' knowledge, studies specialized in analyzing the strengthening effect during the creep process of clay rock are rare.

The ultimate purpose of experimental studies was to interpret the creep mechanism of clayey rock and find a suitable method to establish reliable theoretical models to assess the stability of geological infrastructures. Attempts to establish different classes of constitutive models have been conducted to capture the creep phenomena observed in clayey rocks, and most of these models were based on empirical, rheological, and general stress–strain-time concepts. To interpret the creep behavior of clayey rock, traditional elasto-viscoplastic models have been further developed. Among them, many constitutive models were based on the concept of Perzyna's overstress theory (Perzyna 1966, 1971), e.g., those developed by Kaliakin and Dafalias (1990), Kutter and Sathialingam (1992), Yin and Graham (1994), Modaressi and Laloui (1997), Tang et al. (2008), Yin et al. (2010), and Jiang et al. (2017). However, the main feature of the Perzyna-type models is overstressing, which is closely related to the distance between the viscoplastic yield surfaces and the stress state. The stresses return to the yield surface as a function of time if the external loading remains constant. Still, most of these constitutive models are complicated, involving several parameters.

Valuable research results have been achieved in the study of the creep characteristics of clayey rocks. However, most of the existing experiments were limited to specific clayey rocks, and most of the theories were not universal or were too complicated to determine the related parameters. In this paper, the creep characteristics of clayey rock are first studied through long-term triaxial experiments, and the creep mechanism of clayey rock is analyzed on the microscopic level. A creep constitutive model is established based on Perzyna's overstress theory. This theoretical model is then implemented in the finite element method software ABAQUS FEA by means of subroutine USDFLD. Finally, a three-dimensional (3D) numerical simulation analysis is conducted to better understand the creep behavior of clayey rock and validate the theoretical model.

2 Experimental Study on the Creep Behavior of Clayey Rock

2.1 Experimental Preparation

To study the creep properties of clayey rock, a typical clayey rock was chosen to perform the long-term triaxial compression tests. The main mineral content of this clayey rock was clay minerals, including smectite, illite, and kaolinite, and a considerable main non-clay fraction was present, e.g., quartz and feldspar. Because of

the transversely isotropic properties of this clayey rock, special attention was paid to the sample orientation. The clayey core was trimmed to dimensions of Ø38 × 76 mm with the long axis perpendicular to the strata bedding. The clayey rock had a density of about 2.0 g/cm^3, a porosity of around 40%, and a water content of roughly 20%

Tests were carried out on a multi-field coupled triaxial testing instrument, consisting of a conventional triaxial loading system and a thermal control system. The confining and water pressure were applied by hydraulic pressure generators. The heater coil was installed outside the chamber (Yu et al. (2018). The main parameters of the equipment are listed in Table 1. Both the pressure transducers and the deformation sensor were calibrated, and any possible system error, such as chamber and sample tightness, or internal friction effect, was minimized before the test. The saturation condition of the sample had a significant effect on the creep deformation characteristics of the clayey rock (Lai et al. 2014; Li and Yang 2018), and the focus of this testing was the creep behavior of saturated clayey rocks at ambient temperature. Hence, the main test procedures of the creep tests contain two parts: saturation and creep. For saturation, the clayey rock was drilled under a depth of ~ 200 m. At this level, the in situ stress is approximately 4.5 MPa with a pore pressure of about 2.0 MPa. The clayey samples were saturated under mean effective stress of about 2.5 MPa, corresponding to the in situ mean effective stress. After confirming the saturation of clay samples by checking the Skempton coefficient (> 0.9), the creep stage began at the confining and pore pressures of 4.5 and 2.0 MPa, respectively, under drained conditions. In detail, during creep, the creep load level, i.e., the deviatoric stress, started from 0.5 MPa, followed by loads that increased in stages at 0.5 MPa intervals, and each load level was maintained for one to two months until the sample failed. The main reason for the difference in creep time between the experiments is to analyze the time effect on the strengthening of clayey rock during the creep process. During the experimental study, the temperature of the laboratory was controlled at about 22 ℃.

2.2 Creep behavior of the clayey rock

2.2.1 Creep deformation

Figure 1 shows the deformation and creep-rate variation of the clayey rock during the creep test. The tested clayey rock had a significant creep potential. The creep deformation and creep-rate variation were closely related to the load level. Under a low load level, such as 0.5 or 1.0 MPa, the creep deformation was insignificant, which further confirmed the observation that a creep threshold might exist for clayey rocks. Below this threshold, only primary creep would develop, as proposed by some scholars, like Van Asch Th (1984), Fabre and Pellet (2006), and Zhang et al. (2017). From the test results, the creep threshold for the studied clayey rock was determined to be around 1 MPa. Furthermore, beyond the creep threshold, the increase of the load significantly accelerated the clayey rock deformation. Under a certain load level, the creep deformation coincided with the creep-rate change law. In other words, the creep first experienced a significant growth stage and then transformed into the creep steady-state development stage, and the corresponding creep rate tended to be stable. The green and blue thick dashed lines at the bottom of Fig. 1a roughly show the variation trend of the steady-state creep rate of the samples BCL_1 and BCL_2, respectively. The higher the load level, the higher the creep rate after stabilizing. The samples failed at the load level of 2.5 MPa. The typical deformation and strain rate during the failed stage (take sample BCL_1 for instance) are shown in Fig. 1b. The creep strain rate increased rapidly after a short time decrease when the stress reached 2.5 MPa. Meanwhile, the creep deformation increased infinitely until the sample failed.

The fracture picture of the clayey rock sample BCL_1 is given on the top left of Fig. 1b. The processes involved in a creep are closely related to the microstructural constitution of clayey rocks. The application of external load may arouse the rotation and translation of aggregates accompanied by a breakdown of several particle links, inducing the reorganization of the clay structure and the rearrangement of the interparticle contacts. An orientation of groups of parallel flaky

Table 1 Main technical parameters of the triaxial testing system

Classification	Technical index	Technical parameters	Precision (full-scale percentage)
Axial loading system	Maximum force	50 KN	≤ ± 0.1%
	Axial deformation	0–12 mm	± 0.001 mm
	Radial deformation	0–4 mm	≤ ± 1%
Confining pressure loading system	Confining pressure	0–5 MPa	≤ ± 0.02%
Water pressure loading system	Water pressure	0–5 MPa	≤ ± 0.02%
Temperature controlling system	Temperature	0–100 °C	≤ ± 0.5 °C

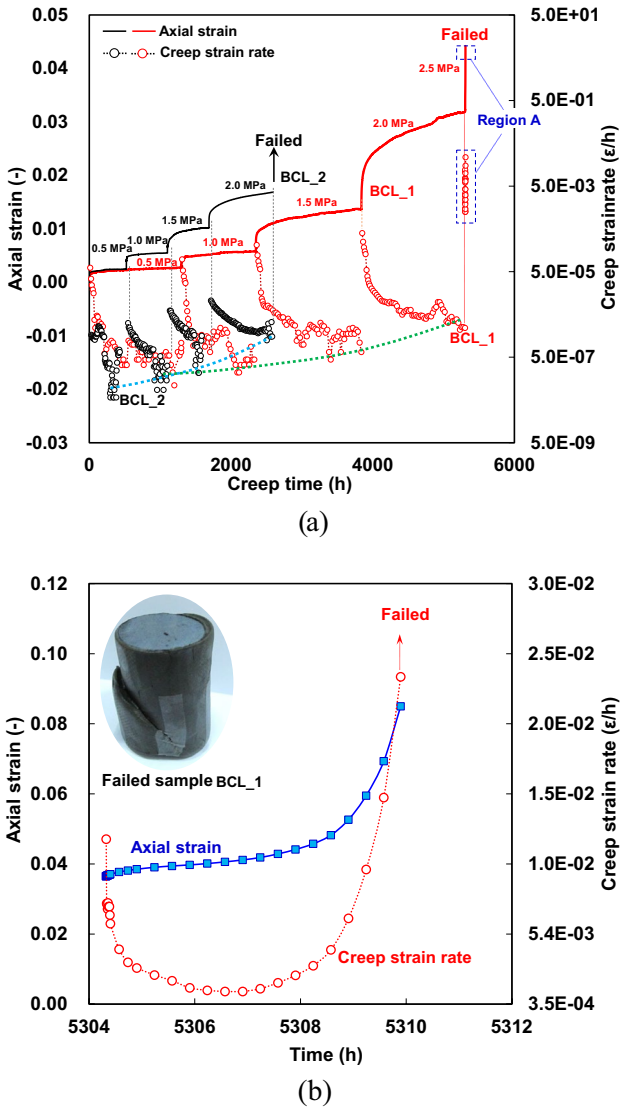

Fig. 1 Creep deformation and creep strain rate versus time **a** global creep deformation and creep strain rate variation and **b** Local enlargement of region A in (**a**) and the failed sample [Note: Each vertical black/red dotted line in (**a**) corresponds to the start or the end of a certain load level]

particles takes place and gradually transforms to slip units. The failed sample contains one main shear plane, which was caused by the development and penetration of the internal fissures promoted by the creep load. The infinite growth of the deformation of the sample after 2.5 MPa implies that under the load level of 2.5 MPa, the specimen slipped along the shear plane and deformed significantly.

2.2.2 Strengthen and Damage During Creep

As aforementioned, the creep process of clayey rock is accompanied by two effects, i.e., strengthening and weakening. The weakening effect during creep for clayey rock is

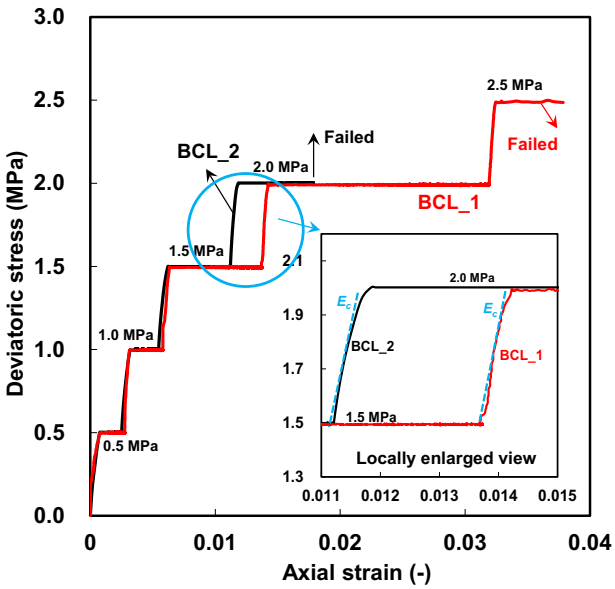

Fig. 2 Stress–strain curve of a clayey rock

generally accepted, and hence, will not be discussed in depth here. Regarding the strengthening effect during the creep process, in terms of macroscopic performance, an analysis of the modulus variation corresponding to the instantaneous deformation of each stage of creep loading provided significant insight. Figure 2 shows the stress–strain curve of a clayey rock during the whole creep process. The obvious creep deformation of the clayey rock is fully displayed in the figure. In choosing the transient loading phases in the stress–strain curve, straight-line segments were selected, and their slopes were taken as the instantaneous elastic moduli (see the detail in the enlarged view in the bottom right). Accordingly, we could find the relationship between the instantaneous elastic modulus E_c and the load level, which is shown in Fig. 3. As indicated in the figure, E_c increased gradually with the increase of the deviatoric stress. The creep time T_c, i.e., the time span for the previous load level before the corresponding elastic modulus is also displayed in Fig. 3. In more detail, for the load level of 2.0 MPa, the creep time T_c is the total creep time under the load level of 1.5 MPa. From the variation law of E_c and T_c, although the elastic modulus for samples BCL_1 and BCL_2 is comparable at the beginning, the subsequent creep time for sample BCL_1 is always longer than that of sample BCL_2 at the same load level, inducing the subsequent elastic modulus variation curve for BCL_1 always above BCL_2, which implies that a longer T_c may result in a larger E_c and more significant strengthening effect inside the clayey rock. We preliminarily deduced that, under a certain load level, although the creep deformation continuously developed, the strengthening effect had a significant advantage over the

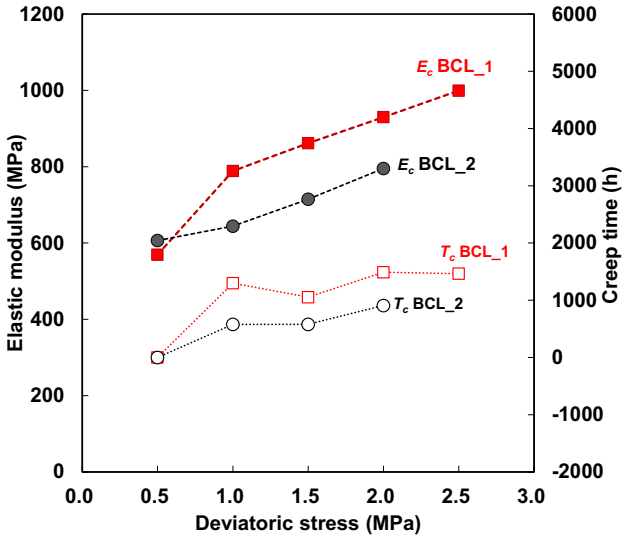

Fig. 3 Elastic modulus E_c and creep time T_c versus deviatoric stress

weakening effect. An accelerated deformation implied that the weakening effect had already exceeded the strengthening effect and might play a dominant role in the subsequent process.

We propose that the turning point where the dominant role of the strengthening and weakening effects changes correlates to the yield stress and creep time of the clayey rock. For the studied clayey rock, under the corresponding stress state of the creep tests in this study, i.e., a mean initial effective stress of 2.5 MPa, a triaxial sheared test showed that the shear strength of the clayey rock was approximately 3.0 MPa, and yield began around 2.0 MPa, about 66% of the peak stress. In addition, the creep time is also a key factor that must be given due attention. At higher loads, if the creep time is long enough, the dominance of the strengthening effect of creep might be threatened. Taking the creep deformation at 2.0 MPa as an example, it can be observed that the creep time of sample BCL_1 is significantly greater than that of BCL_2, resulting in the more significant creep deformation of the sample BCL_1. When the creep time is prolonged indefinitely, particularly in case of tens or hundreds of years, the weakening effect is likely to become dominant, leading to the occurrence of failure.

3 Theoretical Study on the Creep of Clayey Rock

The overstress theory assumes a creep-yield surface exists during the creep process of rock. The stress state during the creep process is not always above the creep yield surface. When the stress state is lower than or on the creep yield surface, the rock does not creep. When the stress exceeds the creep yield surface, the rock begins to creep, and the part of the stress beyond the creep yield surface is called overstress (Perzyna 1966, 1971). During the creep process, the creep yield surface will harden or soften as the creep strain increases, thereby simulating the various stages of creep. The Perzyna overstress theory has the advantages of easy numerical implementation and the ability to describe the time-dependent behavior of geomaterials under complex stress conditions; thus, it has been widely recognized (Yin et al. 2010; Chang and Zoback 2010; Haghighat et al. 2020). Here, we develop a new creep constitutive model based on the overstress theory.

In the elastic-viscoplastic model proposed by Perzyna (1966, 1971), the strain is decomposed into two parts—elastic and viscoplastic. Based on the experimental study on macro- and micro-rheology of clay, Kaliakin and Dafalias (1990) suggested that the irreversible deformation of clay could be divided into time-dependent and -independent parts. In this study, we assume that the strain ε of a clayey rock during creep consists of three parts: elastic strain ε_e, plastic strain ε_p, and creep strain ε_c:

$$\varepsilon = \varepsilon_e + \varepsilon_p + \varepsilon_c \tag{1}$$

The elastic and plastic strain can be determined from the conventional elasto-plastic model. Previous studies have shown that the Drucker–Prager criterion can accurately describe the elasto-plastic behavior of some clayey rocks, e.g., Boom Clay and Opalinus clay (Baldi et al. 1991; François et al. 2011; François and Collin 2017). In this study, we establish theories based on the Drucker–Prager cap model.

3.1 Creep Surfaces

Clayey rocks can yield plastic volumetric strain under hydrostatic pressure. Similarly, the clayey rock may also creep under hydrostatic pressure. Hence, the creep characteristics of clayey rock should consider volumetric creep under hydrostatic pressure in addition to shear creep under deviatoric stress. Thus, we assume two creep mechanisms: cohesion, which follows the type of plasticity active in the shearing yield plasticity region, and consolidation, which follows the type of plasticity active in the cap plasticity region.

When considering the cohesion creep mechanism, the cohesion creep reference surface F_c^s is given by

$$F_c^s = q - \alpha_c p' - k_c = 0, \tag{2}$$

where p' is the effective mean stress, q is deviatoric stress, and α_c and k_c are two creep hardening parameters, where $\alpha_c \le \alpha$ and $k_c \le k$,α and k are the slope and intercept of the shear plane on the $p' - q$ space, respectively, as shown in Fig. 4.

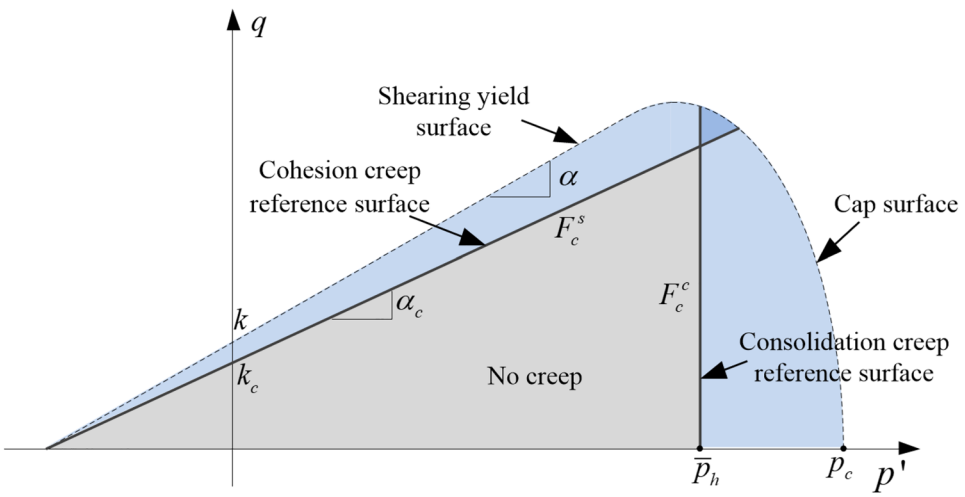

Fig. 4 Regions of activity of creep mechanisms (note: p_c is pre-consolidation pressure)

A simple expression of the consolidation creep reference surface is defined as

$$F_c^c = p - \overline{p}_h = 0, \tag{3}$$

where $\overline{p}_h$ is the creep reference consolidation pressure, which is also a creep hardening parameter. Figure 4 shows the regions of applicability of the creep mechanisms in $p' - q$ space.

We assume that creep iso-inclined surfaces are present, and the equivalent creep surfaces are parallel to the creep reference surfaces, as shown in Fig. 5. A triangular space exists on the meridian surface in which no creep occurs because the equivalent creep stress in this space is zero. Therefore, the equivalent cohesion creep surface can be written as

$$F_c^s = \overline{\sigma}_c - k_c = 0, \tag{4}$$

where $\overline{\sigma}_c = q - \alpha_c p$ is the intersection of the equivalent creep reference surface and the q-axis.

Clearly, the cohesion creep is related to the intersection of the equivalent cohesion creep reference surface and the q-axis, i.e., $\overline{\sigma}_c$. If $\overline{\sigma}_c$ is greater than a threshold value k_c, the cohesion creep is activated. Similarly, the activation of consolidation creep is dependent on whether the intersection point of the equivalent consolidation creep reference surface and the p-axis is beyond the threshold value $\overline{p}_h$.

Thus, the following four cases are included in the model.

Case 1: $p \le \overline{p}_h, \overline{\sigma}_c \le k_c$. No creep is activated.
Case 2: $p > \overline{p}_h, \overline{\sigma}_c \le k_c$. Consolidation creep is activated.
Case 3: $p \le \overline{p}_h, \overline{\sigma}_c > k_c$. Cohesion creep is activated.
Case 4: $p > \overline{p}_h, \overline{\sigma}_c > k_c$. Both cohesion creep and consolidation creep are activated.

3.2 Creep Flow Rules

The cohesion creep G_c^s is assumed to follow a hyperbolic creep potential, as shown in Fig. 6.

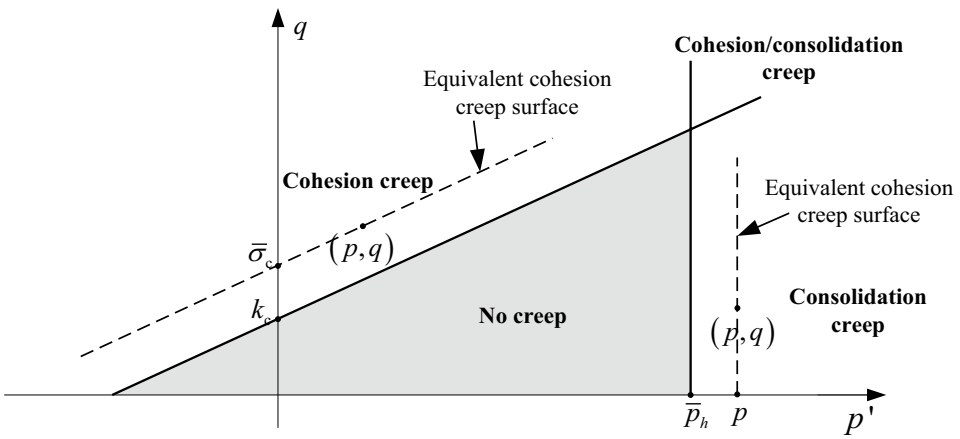

Fig. 5 Schematic diagram of the equivalent creep reference surfaces

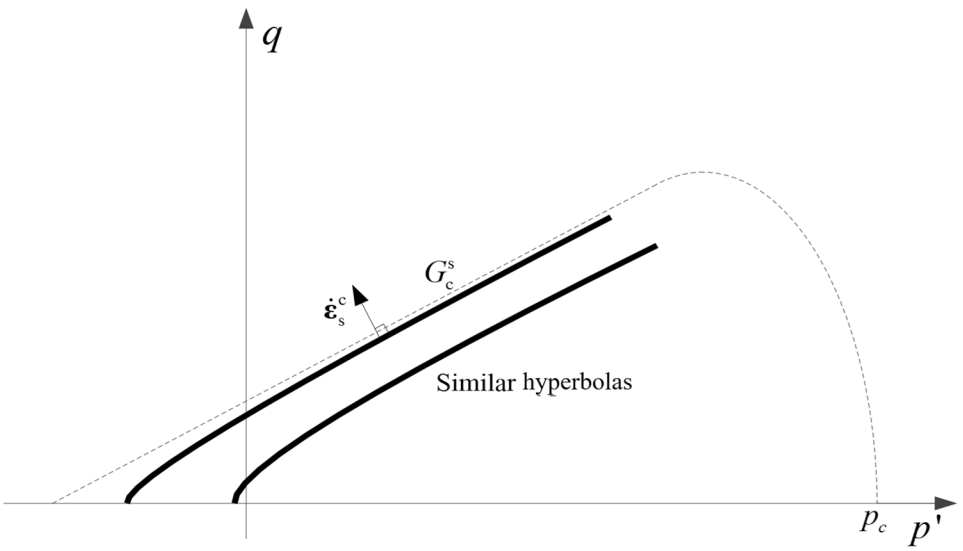

Fig. 6 Schematic diagram of the cohesive creep potential surface

$$G_c^s = \sqrt{\left[\frac{0.1k}{(1-\alpha/3)}\alpha\right]^2 + q^2} - \alpha p. \tag{5}$$

This continuous and smooth creep flow potential ensures that the flow direction is always uniquely defined. The cohesive creep rate $\dot{\boldsymbol{\varepsilon}}_c^s$ is intensity depends on the overstress and can be defined as

$$\dot{\boldsymbol{\varepsilon}}_c^s = \mu_s \left\langle \frac{F_c^s}{f_0} \right\rangle^n \frac{\partial G_c^s}{\partial \boldsymbol{\sigma}} = \mu_s \left\langle \frac{\overline{\sigma}_c - k_c}{f_0} \right\rangle^n \frac{\partial G_c^s}{\partial \boldsymbol{\sigma}}, \tag{6}$$

where $f_0 = 1\,\text{MPa}$ and μ_s is a model parameter. The consolidation creep potential G_c^c, as indicated in Fig. 7, is assumed as follows

$$G_c^c = \sqrt{(p - p_a)^2 + (Rq)^2}, \tag{7}$$

where R is a parameter that controls the geometry of the cap. The consolidation creep rate $\dot{\boldsymbol{\varepsilon}}_c^c$ can be defined as

$$\dot{\boldsymbol{\varepsilon}}_c^c = \mu_c \left\langle \frac{F_c^c}{f_0} \right\rangle^n \frac{\partial G_c^c}{\partial \boldsymbol{\sigma}} = \mu_c \left\langle \frac{p - \overline{p}_h}{f_0} \right\rangle^n \frac{\partial G_c^c}{\partial \boldsymbol{\sigma}}, \tag{8}$$

where μ_c is a model parameter. Thus, the whole creep rate of the clayey rock can be summarized as

$$\dot{\boldsymbol{\varepsilon}}_c^c = \begin{cases} 0 & \text{if } p \le \overline{p}_h, \overline{\sigma}_c \le k_c \\ \mu_c \left\langle \frac{p-\overline{p}_h}{f_0} \right\rangle^n \frac{\partial G_c^c}{\partial \sigma} & \text{if } p > \overline{p}_h, \overline{\sigma}_c \le k_c \\ \mu_s \left\langle \frac{\overline{\sigma}_c - k_c}{f_0} \right\rangle^n \frac{\partial G_c^s}{\partial \sigma} & \text{if } p \le \overline{p}_h, \overline{\sigma}_c > k_c \\ \mu_c \left\langle \frac{p-\overline{p}_E}{f_0} \right\rangle^n \frac{\partial G_c^c}{\partial \sigma} + \mu_s \left\langle \frac{\overline{\sigma}_c - k_c}{f_0} \right\rangle^n \frac{\partial G_c^s}{\partial \sigma} & \text{if } p > \overline{p}_h, \overline{\sigma}_c > k_c \end{cases}. \tag{9}$$

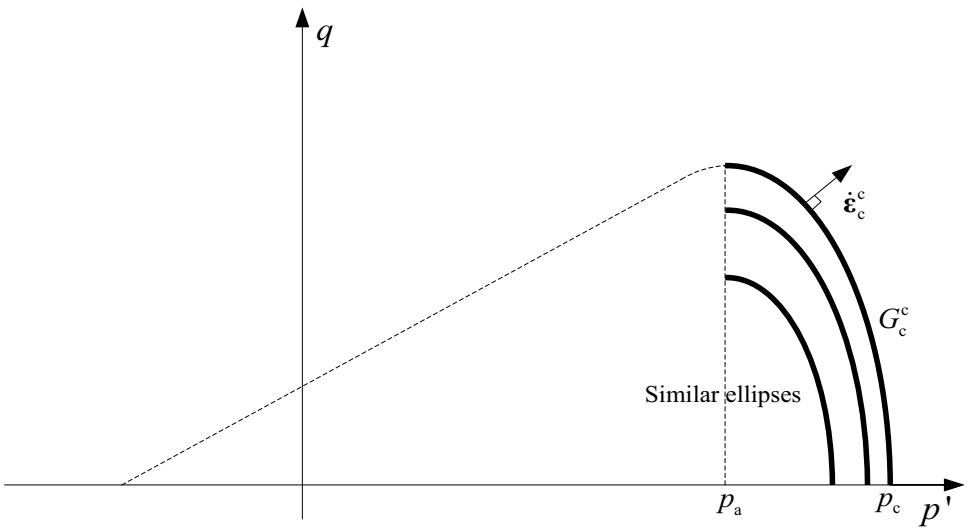

Fig. 7 Schematic diagram of the consolidation creep potential surface

3.3 Creep Hardening and Creep Damage

The analysis in Sect. 2.2.2 shows that the two effects, strengthening and weakening, accompany the creep process of clayey rock. Hence, to describe the creep behavior of clayey rocks, laws considering these two effects should be incorporated into the creep constitutive model. As aforementioned, a creep threshold may exist for clayey rocks. Therefore, the threshold value should ensure the creep reference surface does not surpass the plastic yield surface. The variable for the creep-strengthening effect is assumed to follow a nonlinear hyperbolic rule.

$$h_{\mathrm{c}} = h_{\mathrm{c0}} + \frac{b_{\mathrm{c}}\left(1-h_{\mathrm{c0}}\right)\xi_{\mathrm{c}}}{\left(1-h_{\mathrm{c0}}\right)+b_{\mathrm{c}}\xi_{\mathrm{c}}} \tag{10}$$

in which the equivalent deviatoric creep strain is defined by

$$\begin{cases} \dot{\xi}_{\mathrm{c}} = \sqrt{\frac{2}{3}\dot{\mathbf{e}}_{\mathrm{c}} : \dot{\mathbf{e}}_{\mathrm{c}}} \\ \mathbf{e}_{\mathrm{c}} = \boldsymbol{\varepsilon}_{\mathrm{c}} - \frac{1}{3}tr\left(\boldsymbol{\varepsilon}_{\mathrm{c}}\right)\boldsymbol{\delta} \\ \xi_{\mathrm{c}} = \xi_{\mathrm{c}}\Big|_{0} + \int_{0}^{t}\dot{\xi}_{\mathrm{c}}\mathrm{d}t \end{cases}, \tag{11}$$

where h_{c} is a creep hardening parameter and h_{c0} and b_{c} are model parameters.

Creep damage is introduced to describe the shrinkage of the creep reference surface caused by the accumulation of the creep strain. The evolution of the creep damage factor D_{c} is assumed as

$$D_{\mathrm{c}} = \overline{D}_{\mathrm{c}} - \overline{D}_{\mathrm{c}}\exp\left(-\beta_{\mathrm{c}}\xi_{\mathrm{c}}^{\mathrm{d}}\right), \tag{12}$$

where $\overline{D}_{\mathrm{c}}$ is the upper limit value of D_{c} and d and β_{c} are model parameters.

We assume that the ultimate values of internal creep hardening variables α_{c} and k_{c} are, respectively, equal to α_0 and k_0. Thus, the evolution of α_{c} and k_{c} can be written as

$$\alpha_{\mathrm{c}} = \alpha_0\left(1-D_{\mathrm{c}}\right)h_{\mathrm{c}} \tag{13}$$

$$k_{\mathrm{c}} = k_0\left(1-D_{\mathrm{c}}\right)h_{\mathrm{c}} \tag{14}$$

The evolution law of the threshold value $\overline{p}_{\mathrm{h}}$ is assumed to be

$$\overline{p}_{\mathrm{h}} = \overline{p}_{\mathrm{h0}}\exp\left(c_{\mathrm{ch}}\varepsilon_{\mathrm{c}}^{\mathrm{v}}\right), \tag{15}$$

where the creep volumetric strain is

$$\varepsilon_{\mathrm{c}}^{\mathrm{v}} = \frac{1}{3}tr\left(\boldsymbol{\varepsilon}_{\mathrm{c}}\right). \tag{16}$$

and $\overline{p}_{\mathrm{h0}}$ is the initial value of $\overline{p}_{\mathrm{h}}$ and c_{ch} is a model parameter.

4 Numerical implementation and validation

4.1 Numerical implementation

The finite element method software ABAQUS FEA provides users with a series of subroutines programmed in FORTRAN. The USDFLD subroutine, which updates the parameters, can be used to introduce the hardening or damage law of constitutive models. Meanwhile, the CREEP subroutine allows for the definition of creep laws coupled with rate-independent plastic behavior. By the combined calling of these two subroutines, the proposed creep damage model can be implemented in the ABAQUS platform. The numerical implementation process of the creep constitutive model is shown in Fig. 8.

The calling processes of USDFLD and CREEP subroutine, as shown in Fig. 8, are as follows:

Step 1. Obtain stress, total strain, total strain increment, time increment, and other state variables at the start of the increment from the main ABAQUS program.

Step 2. Update damage variables and modify the model parameters using the USDFLD subroutine.

Step 3. Determine whether the creep is activated. If the creep is activated, calculate the creep strain according to the proposed creep damage model.

Step 4. Calculate the elasto-plastic strain increment.

Step 5. Calculate the elastic trial stress.

Step 6. Return to the main ABAQUS program and perform equilibrium iteration. If the calculation converges, start the next increment. Otherwise, go to Step 1 with a smaller time increment until the calculation converges.

4.2 Numerical Validation

Based on the creep test performed in Sect. 2, a series of back analyses is performed to determine the parameters of the proposed model. To improve the reliability of the back analysis problem and minimize errors between the measured and predicted values, the measured data and inversion models should be combined. Accordingly, we consider it an optimization problem. The Nelder–Mead method, a popular direct search method (Jia 2009; Yu et al. 2014), is thus employed here.

For a certain creep load, the creep strain error between numerical calculations and tests is determined using the least-square method. Back analysis needs to minimize the objective function φ, which is defined as

$$\varphi \rightarrow \min . \tag{23}$$

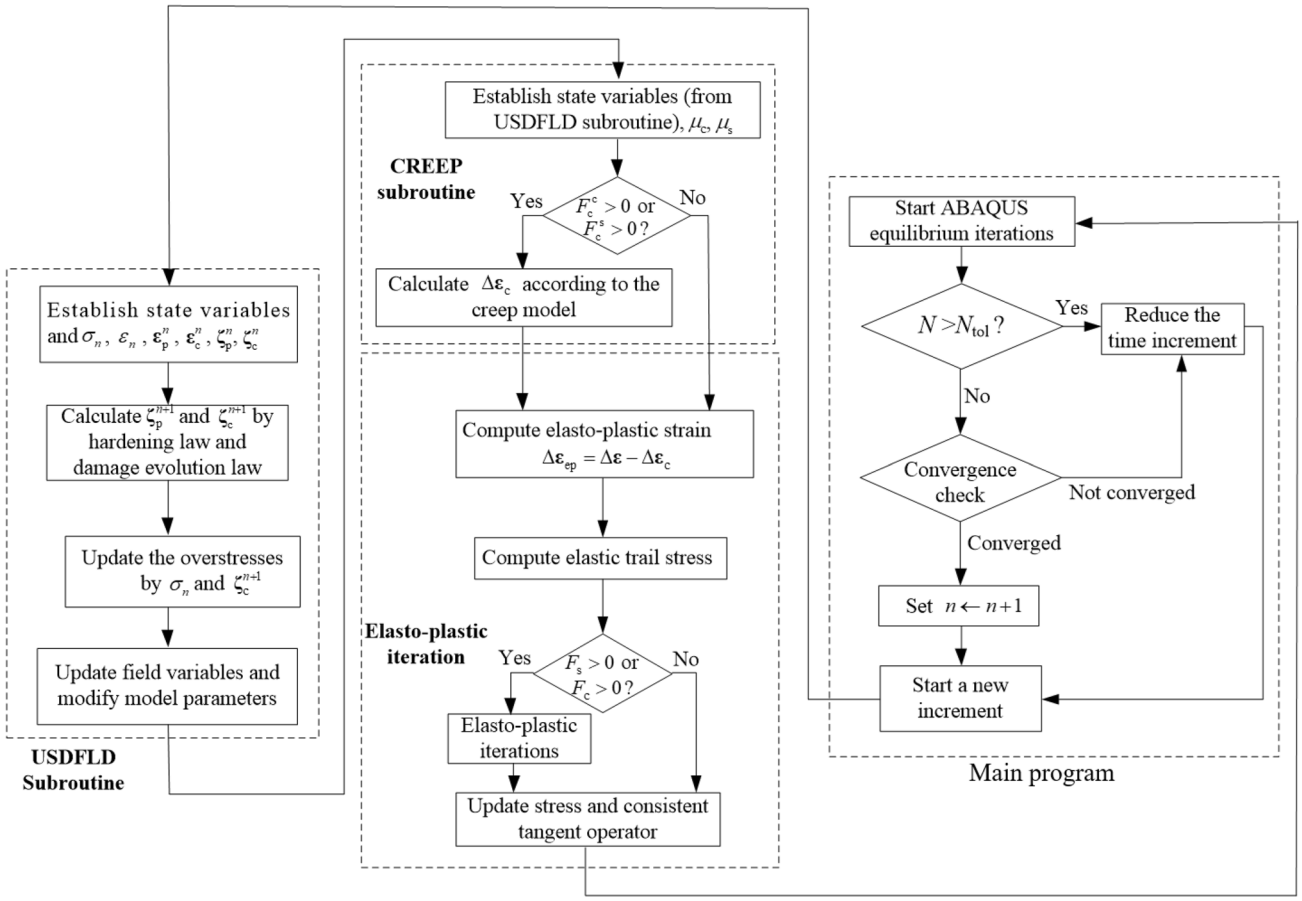

Fig. 8 Numerical implementation of the creep constitutive model (where σ_n,$\varepsilon_n\varepsilon_p^n$, ε_c^n are the total stress, total strain, plastic strain, and creep strain, respectively, at the nth step, ξ_p^n and ξ_c^n are the equivalent plastic and creep strain, respectively, at the nth step, and ξ_p^{n+1} and ξ_c^{n+1} are the equivalent plastic and creep strain, respectively, at the $(n+1)$th step, ε_{eq} is elastic-plastic strain)

The objective function based on the creep strain can be expressed as

$$\varphi\left(n, u_s, \beta_c, d, \overline{D}_c, h_{c0}, b_c, \cdots\right) = \sum_{k=1}^{l}\left(\varepsilon_{cij}^{\text{calk}} - \varepsilon_{cij}^{\text{testk}}\right)^2 \rightarrow \min \tag{24}$$

where $\varepsilon_{cij}^{\text{test}}$ is the (i,j) component of the creep strain obtained by experiments, and $\varepsilon_{cij}^{\text{calk}}$ is the (i,j) component of the creep strain calculated by the back analysis, and l is the number of test data used for back analysis.

Figure 9 shows the 3D finite element model for the clay sample with dimensions of Ø38×76 mm. The bottom of the model is fixed in the axial direction, and the bottom center of the model is fixed in both the axial and radial directions. The boundary conditions and loading step settings for the numerical simulation are the same as those of the creep experiments in Sect. 2. Basic physio-mechanical parameters for the studied clayey rock are listed in Table 2. Table 3 shows the back analysis results for the undetermined parameters.

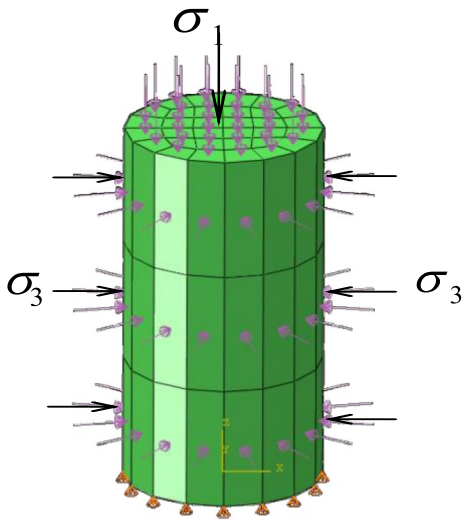

Fig. 9 Schematic diagram of the finite element model for test simulations

Table 2 Basic physio-mechanical parameters for the clayey rock

Parameter	Value
Young's Modulus /MPa	700
Cohesion /MPa	$c_0=0.4$
Friction angle /°	$\varphi_0=15$
Hydraulic conductivity /m·s^{-1}	3×10^{-12}
Poisson's ratio	0.125
Dry density / kg·m^{-3}	1640
Porosity /%	$n_0=39$
Preconsolidation pressure /MPa	5.0

Based on the established 3D finite element model and the determined parameters in Table 3, we simulated the creep tests in Sect. 2. Figure 10 shows the comparison between numerical simulation and experimental results. For the experimental study, although the creep deformation laws of the clayey rock are similar, there are still some differences during the creep due to the internal differences between the two clayey rock samples, such as microstructure, internal defects, etc. In the numerical simulation, the mechanical parameters of the two experiments simulating are same, and the numerical results well reproduce the creep deformation of the sample BCL_2. For the sample BCL_1, the simulation results are slightly different from the test results at the load level of 2.0 MPa, but the change trends are comparable. The comparison between the experimental and numerical study preliminarily confirms the feasibility of the theoretical model applied to the creep analysis of clayey rock. More relevant experimental data are necessary to verify the theoretical model, and further to gain a better understanding of the creep behavior of clayey rock.

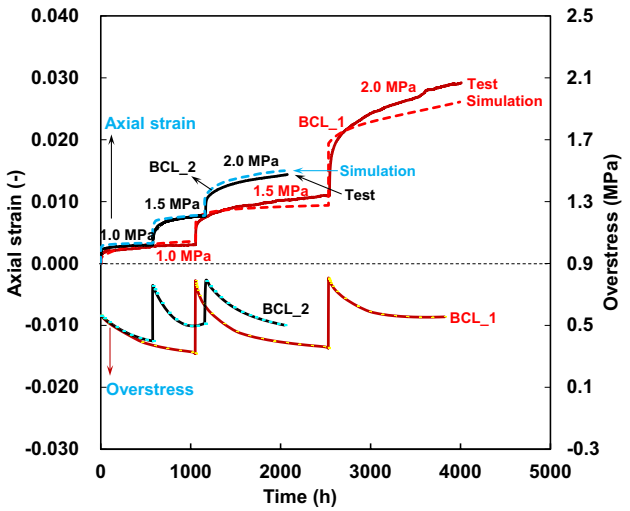

Fig. 10 Comparison between the numerical simulation and test results (Note: the time and axial strain axes were reset.)

Table 3 Parameters of the creep constitutive model for the clayey rock

Parameter	Value	Parameter	Value
n	5	f_0	1
μ_s	5×10^{-5}	$\overline{D}_c$	0.5
μ_c	5×10^{-6}	β_c	2500
h_{c0}	0.2	d	2.5
b_c	180	$\overline{p}_{h0}$/MPa	4.7
c_{ch}	62		

Figure 10 also shows overstress variation during creep. The overstress reaches its maximum at the beginning of each creep stage, then gradually decreases with time and tends to be constant at the end of each creep stage.

5 Conclusion

In this paper, the commonly encountered geomaterial in engineering, clayey rock, is taken as the research object. The creep deformation characteristics of a typical clayey rock under different deviatoric stresses are studied through long-term creep tests. An analysis of the creep mechanism showed that two phenomena, including creep hardening and creep damage, exist in the process of clayey rock creep. The strengthening effect was further verified by analyzing the evolution law of the instantaneous elastic modulus with load levels determined from the instantaneous loading segment. From the experiments, a creep constitutive model was established based on the overstress theory of Perzyna. The model considers the influence of the stress state on the creep yield surface and introduces the laws of hardening and softening. In the end, the theoretical model is validated using the finite element method software ABAQUS FEA, and the reliability of the model is verified by comparing the simulation results with the test results.

Acknowledgements The authors thank the European Underground Research Infrastructure for Disposal of Nuclear Waste in Clay Environment (EURIDICE) for collaborating on the long-term HM behavior of Boom Clay. Owing to this international cooperation, we could perform the research in this paper. The financial support of the National Natural Science Foundation of China (No. 51879258, 51979266, and 51991392) is greatly acknowledged. Appreciations are extended to Sweetland K, who has given valuable suggestions and worked hard on improving the English of this article.

Declarations

Conflict of interest The authors declare that the aforementioned contents represent their personal opinions and not the opinions of other organizations or individuals.

Data availability statement The data that support the findings of this study are available from the corresponding author upon reasonable request.

References

Arulanandan K, Shen CK, Young RB (1972) Discussion: Undrained creep behaviour of a coastal organic silty clay. Géotechnique 22(3):536–537

Baldi G, Hueckel T, Peano A, Pellegrini R (1991) Developments in modelling of thermohydro-geomechanical behaviour of Boom Clay and clay-based buffer materials (volume 2) (No. EUR-13365/2). Commission of the European Communities

Blümling P, Bernier F, Lebon Pm Martin CD (2007) The excavation damaged zone in clay formations time-dependent behaviour and influence on performance assessment. Phys Chem Earth 32(8–14):588–599

Bonini M, Barla G, Barla M (2003) Characterisation studies of Tectonised Clay Shales and implications in the excavation of large size tunnels[C]//ISRM 2003–Technology roadmap for rock mechanics, South African Institute of Mining and Metallurgy

Chang CD, Zoback MD (2009) Viscous creep in room-dried unconsolidated Gulf of Mexico shale (I): experimental results. J Pet Sci Eng 69:239–246

Chang CD, Zoback MD (2010) Viscous creep in room-dried unconsolidated Gulf of Mexico shale (II): Development of a viscoplasticity model. J Pet Sci Eng 72(1–2):50–55

Desbois G, Höhne N, Urai JL, Bésuelle P, Viggiani G (2017) Deformation in cemented mudrock (Callovo-Oxfordian Clay) by microcracking, granular flow and phyllosilicate plasticity: insights from triaxial deformation, broad ion beam polishing and scanning electron microscopy. Solid Earth 8(2):291–305

Fabre G, Pellet F (2006) Creep and time-dependent damage in argillaceous rocks. Int J Rock Mech Min 43(6):950–960

François B, Collin F (2017) Anisotropic modelling of Opalinus Clay behaviour: from triaxial tests to gallery excavation application. J Rock Mech Geotech 9(3):435–448

François B, Collin F, Dizier A, Charlier R (2011) An extended Drucker-Prager hardening model for cross-anisotropy of soft rocks. In: Proceedings of the 15th European Conference on Soil Mechanics and Geotechnical Engineering, pp 537–540

Gasc-Barbier M, Chanchole S, Bérest P (2004) Creep behavior of Bure clayey rock. Appl Clay Sci 26(1–4):449–458

Giraud A, Rousset G (1996) Time-dependent behaviour of deep clays. Eng Geol 41:181–195

Griggs DT (1939) Creep of rocks. J Geol 47:225–251

Haghighat E, Rassouli FS, Zoback MD, Juanes R (2020) A viscoplastic model of creep in shale. Geophysics 85(3):155–166

Jia SP (2009) Hydro-mechanical coupled creep damage constitutive model of Boom clay, back analysis of model parameters and its engineering application. Institute of Rock and Soil Mechanics, Chinese Academy of Sciences, Wuhan

Jiang JH, Ling HI, Kaliakin VN (2017) On a damage law for creep rupture of clays with accumulated inelastic deviatoric strain as a damage measure. Mech Res Commun 83:22–26

Kaliakin VN, Dafalias YF (1990) Theoretical aspects of the elastoplastic-viscoplastic bounding surface model for cohesive soils. Soils Found 30(3):11–24

Kupferschmied N, Wild KM, Amann F, Nussbaum Ch, Jaeggi D, Badertscher N (2015) Time-dependent fracture formation around a borehole in a clay shale. Int J Rock Mech Min 77:105–114

Kutter BL, Sathialingam N (1992) Elastic-viscoplastic modelling of the rate-dependent behaviour of clays. Geotechnique 42(3):427–441

Lai XL, Wang SM, Ye WM, Cui YJ (2014) Experimental investigation on the creep behavior of an unsaturated clay. Can Geotech J 51(6):621–628

Li J, Yang Y (2018) Creep behavior of unsaturated reticulate red clay under matric suction. KSCE J Civ Eng 22:582–587

Liu ZB, Xie SY, Shao JF, Conil N (2015) Effects of deviatoric stress and structural anisotropy on compressive creep behavior of a clayey rock. Appl Clay Sci 114:491–496

Modaressi H, Laloui L (1997) A thermo-viscoplastic constitutive model for clays. Int J Numer Anal Met 21(5):313–335

Naumann M, Hunsche U, Schulze O (2007) Experimental investigations on anisotropy in dilatancy, failure and creep of Opalinus Clay. Phys Chem Earth 32:889–895

Neerdael B, De Bruyn D, Mair RJ, Taylor RN (1999) Geotechnical behavior of Boom Clay. Commission of the European Communities, Nuclear Science and Technology, Pilot tests on radioactive waste disposal in underground facilities, EUR 13985EN, pp 223–238

Perzyna P (1966) Fundamental problems in viscoplasticity. Adv Appl Mech 9:243

Perzyna P (1971) Thermodynamic theory of viscoplasticity. Adv Appl Mech 11:313–354

Pusch R (1979) Creep mechanisms in clay. Mechanisms of Deformation and Fracture, Pergamon. In: Proceedings of the Interdisciplinary Conference held at the University of Luleå, Luleå, Sweden, September 20–22, 1978, pp 351-359

Pusch R, Knutsson S, Liu Xd, Yang T (2016) Creep can strengthen clay: a matter of long-term slope stability. J Earth Sci Geotech Eng 6(1):1–18

Robinet JC, Sardini P, Coelho D, Parneix JC, Prêt D, Sammartino S, Boller E, Altmann S (2012) Effects of mineral distribution at mesoscopic scale on solute diffusion in a clay-rich rock: example of the Callovo-Oxfordian mudstone (Bure, France). Water Resour Res 48:W05554

Shi X, Yang X, Yue W, Yang L, Gui J, Huang H, Jiang S (2022) Experimental investigation on the creep behaviors of shale using nanoindentation technique and fractional constitutive models. J Pet Sci Eng. https://doi.org/10.1016/j.petrol.2022.110520

Tang AM, Cui YJ, Tali B, Doan DH (2008) Etude du comportement thermo-hydro-mécanique visqueux de l'argile de Boom[R]. École des Ponts Paris Tech, Paris

Van Asch Th WJ (1984) Creep processes in landslides. Earth Surf Proc Land 9(6):573–583

Vu M, Souley M, Alonso M, Vaunat J, Gens Solé A, Plúa C, de Lesquen C, Armand G (2021) Creep effects on the thermo-hydro-mechanical responses of Callovo-Oxfordian claystone. In: A: "Challenges and Innovations in Geomechanics: Proceedings of the 16th International Conference of IACMAG". Berlín: Springer, pp 663–671

Wang H, Jiang C, Zheng PQ, Li N, Zhan YB (2020) Deformation and failure mechanism of surrounding rocks in crossed-roadway and its support strategy. Eng Fail Anal 116:104743

Yang SQ, Jing HW, Cheng L (2014) Influences of pore pressure on short-term and creep mechanical behavior of red sandstone. Eng Geol 179:10–23

Yang SQ, Xu P, Ranjith PG (2015) Damage model of coal under creep and triaxial compression. Int J Rock Mech Min 80:337–345

Yin JH, Graham J (1994) Equivalent times and one-dimensional elastic viscoplastic modelling of time-dependent stress-strain behaviour of clays. Can Geotech J 31(1):42–52

Yin ZY, Chang CS, Karstunen M, Hicher PY (2010) An anisotropic elastic-viscoplastic model for soft clays. Int J Solids Struct 47(5):665–677

Yu HD, Chen WZ, Li XL, Sillen X (2014) A Transversely isotropic damage model for boom clay. Rock Mech Rock Eng 47(1):207–219

Yu HD, Chen WZ, Gong Z, Tan XJ, Ma YS, Li XL, Sillen X (2015) Creep behavior of Boom clay. Int J Rock Mech Min 76:256–264

Yu HD, Chen WZ, Gong Z, Ma YS, Chen GJ, Li XL (2018) Influence of temperature on the hydro-mechanical behavior of Boom Clay. Int J Rock Mech Min Sci 108:189–197

Yu HD, Lu C, Chen WZ, Tian HM (2021) An insight into the creep mechanisms of a clayey soil through long-term consolidation tests. Bull Eng Geol Environ 80:9127–9139

Zeng LB, Zhao JY, Zhu SJ, Xiong WJ, He YH, Chen JW (2008) Impact of rock anisotropy on fracture development. Prog Nat Sci 18(11):1403–1408

Zhang CL, Laurich B (2020) Mechanical behavior of sandy facies of Opalinus Clay under different load conditions. J Rock Mech Geotech 12:223–241

Zhang CL, Rothfuchs T (2004) Experimental study of the hydro-mechanical behaviour of the Callovo-Oxfordian argillite. Appl Clay Sci 26(1–4):325–336

Zhang XW, Wang CM, Li JX, Ma DH, Chen DC (2010) Variation characteristics of soft clay micropore in creep condition. Rock Soil Mech 31(4):1061–1067

Zhang F, Tang YS, Liu ZB, Shao JF, Sheng Q, Zhou H (2017) Experimental study on creep rate thresholds of COx clay rock under triaxial compression. J Rock Mech Eng 36(03):644–649

Zhao D, Gao QF, Hattab M, Hicher PY, Yin ZY (2020) Microstructural evolution of remolded clay related to creep. Transp Geotech 24:100367